Classical and quantum phase transitions in the Lipkin-Meshkov-Glick model

Octavio Castaños, Ramón López-Peña, and Jorge G. Hirsch
Instituto de Ciencias Nucleares Universidad Nacional Autónoma de México, Apartado Postal 70-543, México 04510 D.F.

Enrique López-Moreno
Departamento de Física, Facultad de Ciencias Universidad Nacional Autónoma de México, Apartado Postal 70-542, México 04510 D.F.

(Received 18 November 2005; revised manuscript received 21 March 2006; published 28 September 2006)

An analysis of the classical and quantum phase transitions of the Lipkin-Meshkov-Glick model is presented. It is shown that the classical dynamics is ruled by the energy surface of the system. Applying the catastrophe formalism to this energy surface the separatrix is obtained. It determines the regions in the control parameter space where there are phase transitions. Special attention is given to the compositions of ground and first-excited energy states, which are well described by the even and odd SU(2) coherent states. Phase transitions are shown to be associated with a change in the wave functions from collective to single-particle behavior. Evaluating the distribution of nearest-neighbor spacings it is shown that the separatrix of the system emerges as a useful tool to describe the global behavior of the quantum-level structure and their corresponding wave functions.

DOI: 10.1103/PhysRevB.74.104118 PACS number(s): 05.70.Fh, 03.65.Fd, 21.60.Fw, 42.50.Dv

I. INTRODUCTION

Spin squeezing has been receiving a great deal of attention both for the fact that it exhibits reduced fluctuations below the fundamental spin noise in collections of atoms and for the possibility of using it as a measure of entanglement in multiatom systems.[1]

The Lipkin-Meshkov-Glick (LMG) model Hamiltonian, in the field of quantum optics, allowed Kitagawa and Ueda[2] the generation of spin-squeezed states. It appears as an effective Hamiltonian yielding a multiparticle entangled state,[3] or in the formation of entangled states of two-mode Bose-Einstein condensates[4] and, in some works, as a superposition of two mesoscopic distinguishable states.[5]

Since the beginning of the 1980s,[6] it has been known that the LMG model represents an approximation to ferromagnetic Ising models and by means of a semiclassical approach that has second-order phase transitions in the limit of a large number of particles. Phase transitions at the large-N limit have been also studied more recently.[7–9] In these works, analytical or numerical determinations of finite-size scaling exponents for thermodynamical quantities such as the energy spectrum are established. In general, it has been found that spin squeezing is a sufficient but not necessary condition for entanglement, with different definitions of spin squeezing giving also different predictions of entanglement in the two-atom Dicke systems.[10]

In the interacting boson model of the nuclei,[11,12] it has been established that energy surfaces generated from the most general one- and two-body central interactions have only two essential control parameters.[13] The classical theory of phase transitions within the catastrophe formalism[14,15] demonstrates that the associated energy surfaces can have shape phase transitions of zero, first, and second order.[13] In this procedure, one considers the deformation parameters β and γ of the energy surface as the order parameters. A shape phase transition occurs when the control parameters of the Hamiltonian are varied and the deformation variables jump from one critical branch to another. Quantum phase transitions between spherical, prolate, oblate, and γ-unstable nuclear ground-state shapes have been found in the interacting boson model (IBM),[16] with an analogy between the IBM results and predictions of the Landau theory of phase transitions in classical thermodynamics.[17–19]

A characterization of phase transitions and related accidental degeneracies associated with the LMG model Hamiltonian by means of its associated separatrix was presented in Ref. 20. Besides, for the first time the associated degeneracies of the LMG model Hamiltonian were presented in analytical form, as hyperbolas indicating the regions, in the Hamiltonian parameters space, where there are degeneracies between the energy levels.

In this contribution a detailed analysis of the behavior of the classical trajectories and quantum properties in the vicinity of the separatrix is presented. The composition of the exact even and odd quantum solutions is compared with the standard, even, and odd spin coherent states. Thus, the regions in the control parameter space where the standard, even, and odd spin coherent states best describe the ground and first-excited states of the LMG model are established. Also the distribution of nearest-neighbor spacings of the energy levels, the expectation value of the distribution of particles between the levels, and its corresponding fluctuations are determined. The separatrix divides the parameter space into three regions where the ground state exhibits quite different Dicke-state compositions. In nuclear physics they are associated with either single-particle or collective behavior. In optics they are related to the distribution of occupancies of two-level atoms, ranging from all the atoms in the lower level to atoms equally distributed in both levels. In the ferromagnetic Ising model the magnetization and the gap[6] exhibit a behavior which is closely related with the expectation values of the population of the excited states in the two-level

atom analyzed in this work. The asymptotic limit of the expectation value of the population operator is studied for a very large number of particles. In this limit the standard spin coherent state provides a very good approximation for the exact solution.

In Sec. II a brief review of the model Hamiltonian and a detailed analysis of the geometric interpretation of the model is presented, starting with the definition of standard, even, and odd spin coherent states. The corresponding energy surfaces are evaluated, which provide the Hartree-Fock descriptions of the ground and first-excited states. Afterwards the bifurcations and Maxwell sets are obtained, classifying the regions in the control parameter space where there are phase transitions in the energy surfaces. Through a time-dependent variational principle the classical dynamical behavior of the system is analyzed. In Sec. IV, a comparison of the composition of the exact even and odd quantum solutions with those associated to the standard, even, and odd coherent states, in the vicinity of the separatrix, is presented. Besides, the behavior of the expectation value of the population operator for a large number of particles and the nearest-neighbor spacings of the energy levels in a region of the control parameter space are presented. Finally the conclusions are given.

II. LIPKIN-MESHKOV-GLICK MODEL

The LMG model was conceived as a test model in nuclear physics. It is simple enough to be solved exactly but it is yet nontrivial. For that reason, since it was established[21] has been used to validate many fermion approximation methods like Hartree-Fock[22] and the random phase approximation (RPA).[23] The LMG model assumes that the nucleus is a system of fermions which can occupy two levels with the same degeneracy Ω, separated by an energy ϵ. It can also describe a system of interacting two-level atoms, or an anisotropic XY Ising model in a transverse field with infinite-range constant interactions.[6] There are residual interactions which scatters pairs of particles between the two levels without changing the total number of particles occupying the shells. In the quasispin formalism the model Hamiltonian is[21]

$$H = \epsilon J_0 + \frac{\lambda}{2}(J_+^2 + J_-^2) + \frac{\gamma}{2}(J_+J_- + J_-J_+). \tag{1}$$

The angular momentum operators are realized in terms of fermion creation $c_{\alpha n}^\dagger$ and annihilation operators $c_{\alpha n}$:

$$J_0 = \frac{1}{2}\sum_{n=1}^{\Omega}(c_{+n}^\dagger c_{+n} - c_{-n}^\dagger c_{-n}),$$

$$J_+ = \sum_{n=1}^{\Omega} c_{+n}^\dagger c_{-n}, \quad J_- = \sum_{n=1}^{\Omega} c_{-n}^\dagger c_{+n}. \tag{2}$$

The index $\alpha = \pm$ denotes the lower and upper single-particle levels. These operators are the generators of the algebra of the SU(2) group. Thus, in Hamiltonian (1), the λ term annihilates pairs of particles in one level and creates pairs in the other level while the γ term scatters one particle up while another is scattered down.

Exact eigenvalues and eigenvectors of the Hamiltonian (1) can be obtained in the Dicke basis states:

$$|Nn\rangle = \sqrt{\frac{(N-n)!}{(N)!\,(n)!}} J_+^n |N0\rangle, \tag{3}$$

where $n = j + m$ takes values between 0 and N. The state $|N0\rangle$ is the unperturbed ground state—i.e., the ground state when $\lambda = \gamma = 0$, where all the particles occupy the lowest energy level.

The eigenvalue equation for the system is easily solved by diagonalizing the matrix Hamiltonian. As a reflection of its parity symmetry, Hamiltonian (1) has only nonvanishing matrix elements between states (3) with $n \to n$ and $n \pm 2$. The Hamiltonian matrix is broken into two blocks, each one associated with the parity of the number of particle-hole pairs, n. For this reason the eigenfunctions can be written in terms of linear combinations of states with even (e) or odd (o) values of n: namely,

$$|s,e\rangle = \sum_{i=1}^{\lceil (N+1)/2 \rceil} C_{i,e}^s |N2i-2\rangle,$$

$$|s',o\rangle = \sum_{i=1}^{\lfloor (N+1)/2 \rfloor} C_{i,o}^{s'} |N2i-1\rangle, \tag{4}$$

where the eigenvalue running indices take the values $s = 1, 2, \ldots, \lceil (N+1)/2 \rceil$ and $s' = 1, 2, \ldots, \lfloor (N+1)/2 \rfloor$. In these expressions, the last terms indicate the minimum integer that contains $(N+1)/2$ and the maximum integer which is contained by $(N+1)/2$, respectively.

III. CLASSICAL ANALYSIS

We study the geometric interpretation of the nonlinear spin Hamiltonian (1). The classical limit of this system is established by studying the expectation value of the Hamiltonian in the SU(2) coherent states. This expectation value defines the energy surface, and it is analyzed using the catastrophe theory formalism. Once the critical points are found, it is necessary to determine which of them belong to bifurcation or Maxwell sets. The union of these sets is the *separatrix* of the system, which classifies the regions in the essential parameters space where there are phase transitions. The order of these transitions is determined according to the thermodynamic Ehrenfest classification.

A. Standard, even, and odd SU(2) coherent states

We use as trial states the normalized SU(2) coherent states, which are defined as[24]

$$|\zeta\rangle = (1 + |\zeta|^2)^{-j} |\zeta\}$$
$$= (1 + |\zeta|^2)^{-j} \exp(\zeta^* J_+) |N,0\rangle, \tag{5}$$

where $|\zeta\}$ is the non-normalized spin coherent state, which will play a fundamental role in defining a classical mechanics, and the unperturbed ground state $|N,0\rangle$ was defined in

the previous section. The variable ζ represents a point in the complex plane mapped by the stereographical projection of a point on the sphere from its south pole,

$$\zeta = \frac{x+iy}{1+z} = \tan(\theta/2)\exp(i\phi), \tag{6}$$

where x, y, and z are the Cartesian coordinates of a point over the surface of the unit sphere, and θ and ϕ are its polar and azimuthal angles, respectively.

These trial coherent states mix states with odd and even powers of the number of particle-hole pairs, which are never mixed in the exact eigenstates (4), due to the *parity* symmetry discussed in the previous section. Trial states with good parity properties can be built as even and odd coherent states $|\pm\rangle$,[25]

$$|\zeta\rangle_{\pm} = \mathcal{N}_{\pm}(|\zeta\rangle \pm |-\zeta\rangle), \tag{7}$$

where $\mathcal{N}_{\pm}$ are their normalization functions, defined as

$$\mathcal{N}_{\pm} = \frac{\sqrt{(1+|\zeta|^2)^{2j}}}{\sqrt{2[(1+|\zeta|^2)^{2j} \pm (1-|\zeta|^2)^{2j}]}} = \frac{1}{\sqrt{2[1 \pm (\cos\theta)^{2j}]}}. \tag{8}$$

The expectation value of the Hamiltonian between coherent states is given by

$$E(\theta,\phi) = \langle\zeta|H|\zeta\rangle. \tag{9}$$

For given values of the Hamiltonian parameters, it represents the *classical energy surface*. After making a shift and a magnification, the expectation value of the Hamiltonian between coherent states can be written as[26]

$$\mathcal{E}(\theta,\phi) = \frac{\langle\zeta|H|\zeta\rangle - \gamma j}{\omega j} = -2\cos\theta + \gamma_x \sin^2\theta\cos^2\phi + \gamma_y \sin^2\theta\sin^2\phi, \tag{10}$$

where the parameters γ_x and γ_y are defined by

$$\gamma_x = \frac{2j-1}{2\omega}(\gamma+\lambda), \quad \gamma_y = \frac{2j-1}{2\omega}(\gamma-\lambda). \tag{11}$$

The expectation values of the Hamiltonian between even (e) and odd (o) spin coherent states take the form

$$\mathcal{E}_{e/o}(\theta,\phi) = \frac{{}_{e/o}\langle\zeta|H|\zeta\rangle_{e/o} - \gamma j}{\omega j} = \mathcal{E}(\theta,\phi)F_{e/o}(\theta,j) \mp (\gamma_x+\gamma_y)G_{e/o}(\theta,j), \tag{12}$$

where the functions F, G are given by the expressions

$$F_{e/o}(\theta,j) = \frac{1 \pm (\cos\theta)^{2j-2}}{1 \pm (\cos\theta)^{2j}},$$

$$G_{e/o}(\theta,j) = \frac{(\sin\theta)^2(\cos\theta)^{2j-2}}{1 \pm (\cos\theta)^{2j}}. \tag{13}$$

The same shift and magnification are chosen for the three energy surfaces to allow a simple comparison between them. When $j \to \infty$, the functions $F_{e/o}$ go to the unity and functions $G_{e/o}$ go to zero. The functions $\mathcal{E}$, $\mathcal{E}_e$, and $\mathcal{E}_o$ are called standard, even, and odd energy surfaces. In the asymptotic limit $j \to \infty$ they are all equivalent.

Besides energy surfaces we can also evaluate other properties like the probability amplitude of the number of particle-hole pairs, together with its corresponding probability distribution function which is related to the population of the two-level system. Thus for the spin coherent states we get

$$P(n) = |\langle Nn|\zeta\rangle|^2 = \frac{N!}{(N-n)!\,n!}\left(\frac{1+z}{2}\right)^{N-n}\left(\frac{1-z}{2}\right)^{n}, \tag{14}$$

where $z=\cos\theta$ and $P(n)$ is the probability of finding the coherent state $|\zeta\rangle$ in the Dicke state $|Nn\rangle$. This is a binomial distribution where $p \equiv (1+z)/2$ is the probability of finding one particle in the ground-state level, while $q \equiv (1-z)/2$ is the corresponding probability of finding a particle in the excited level.

For the even and odd spin coherent states the probability distribution function of particle-hole pairs is given by

$$P_{e/o}(n) = \frac{1 \pm (-1)^n}{1 \pm z^N} P(n), \tag{15}$$

where the distribution function is zero if the number of particle-hole pairs is odd, for even spin coherent state, or even, for odd spin coherent state.

The expectation value of J_0 is related with the population of particles in the excited state of the two-level system. Thus the expectation value of the operator of the number of particles in the upper level, which we called from here on the population operator,

$$\hat{n} = N/2 + J_0,$$

and its fluctuation $\Delta\hat{n}$ are calculated for the standard, even, and odd spin coherent states. The results for the expectation value for the population operator are the following:

$$\langle\zeta|\hat{n}|\zeta\rangle = j(1-z),$$

$${}_{e/o}\langle\zeta|\hat{n}|\zeta\rangle_{e/o} = j\left\{1 - z\frac{1 \pm z^{2j-2}}{(1 \pm z^{2j})^2}\right\}, \tag{16}$$

where for the odd spin coherent state, when $z \to 1$, the appropriate limits of the given expression must be taken into account.

To determine the fluctuations of the population number operator, it is necessary to calculate the expectation value of $\hat{n}^2$ with respect to the standard, even, and odd spin coherent states. The corresponding expressions are

$$\langle\zeta|\hat{n}^2|\zeta\rangle = j^2(1-z)^2 + \frac{j}{2}(1-z^2),$$

$$_{elo}\langle\zeta|\hat{n}^2|\zeta\rangle_{elo} = j\left(j+\frac{1}{2}\right) - \frac{2j^2z}{1\pm z^{2j}}(1\pm z^{2j-2}) + \frac{j(2j-1)z^2}{2(1\pm z^{2j})}\{1\pm z^{2j-4}\}, \quad (17)$$

where again the odd case must be simplified properly when the limit $z\to 1$ is taken.

B. Separatrix

A complete analysis of the normal energy surface (10), when the control parameters γ_x and γ_y are varied, allows the determination of critical points, their degeneracy, the bifurcation sets of the energy surface, and the loci in the control parameters space at which a phase transition occurs from one local critical point to another. One can organize all the critical points according to their stability within the control parameter space.

The analysis of the critical points of the energy surface is simpler if we use Cartesian coordinates:

$$x = \sin\theta\cos\phi, \quad y = \sin\theta\sin\phi,$$

$$z = \cos\theta.$$

In these coordinates the standard energy surface takes the form

$$\mathcal{E}^{\pm}(x,y) = \mp 2\sqrt{1-x^2-y^2} + \gamma_x x^2 + \gamma_y y^2, \quad (18)$$

where both signs—i.e., negative and positive values of z—must be included to describe the motion on the sphere.

The dynamical behavior of the system is determined with the knowledge of the critical points and their Hessian matrix $\mathcal{H}_{ij}$, built with the second derivatives of energy—i.e.,

$$\nabla\mathcal{E}^{\pm}(x,y;\gamma_x,\gamma_y) = 0,$$

$$\mathcal{H}^{\pm}_{ij} =: \left.\frac{\partial^2\mathcal{E}^{\pm}}{\partial x_i\,\partial x_j}\right|_{(x_1=x^c,x_2=y^c)}, \quad (19)$$

where the superscript denotes a critical point for the variables.

In Table II of the Appendix, the critical points of the function $\mathcal{E}^+$ are given together with its nature—i.e., if they are maxima, minima, or saddle points. Next, the bifurcation sets of the function $\mathcal{E}^+$ are obtained from the condition $\det\mathcal{H}_{ij}=0$, for each critical point.

(i) $(x_c,y_c)=(0,0)$: In this critical point, the elements of the Hessian matrix are

$$\mathcal{H}^+_{xx} = 2(1+\gamma_x), \quad \mathcal{H}^+_{xy} = 0, \quad \mathcal{H}^+_{yy} = 2(1+\gamma_y).$$

The condition $\det\mathcal{H}=0$ yields the bifurcation sets

$$\gamma_x = -1 \quad \text{and} \quad \gamma_y = -1. \quad (20)$$

This critical point is a minimum if $\gamma_x>-1$ and $\gamma_y>-1$, while it is a maximum if $\gamma_x<-1$ and $\gamma_y<-1$. Otherwise it is a saddle point.

TABLE I. In the first column the critical points of the function $\mathcal{E}(\theta,\phi)$ in Cartesian coordinates are given, while in the second one, the corresponding critical points in terms of θ and ϕ are established.

(x_c,y_c)	(θ_c,ϕ_c)
$(0,0)$	$(0,0)$ and $(\pi,0)$
$(\pm x_c,0)$	$(\theta_c,0)$ and (θ_c,π)
$x_c=\sqrt{1-1/\gamma_x^2}$	$\theta_c=\arccos(-1/\gamma_x)$
$(0,\pm y_c)$	$(\theta_c,\pi/2)$ and $(\theta_c,3\pi/2)$
$y_c=\sqrt{1-1/\gamma_y^2}$	$\theta_c=\arccos(-1/\gamma_y)$
$\gamma_x=\gamma_y=\gamma_0$	
(x_c,y_c)	(θ_c,ϕ)
$x_c^2+y_c^2=1-1/\gamma_0^2$	$\theta_c=\arccos(-1/\gamma_0)$

(ii) $(x_c,y_c)=(\pm\sqrt{1-1/\gamma_x^2},0)$ and $\gamma_x<-1$: Now the elements of the Hessian matrix are

$$\mathcal{H}^+_{xx} = 2\gamma_x(1-\gamma_x^2) > 0, \quad (21)$$

$$\mathcal{H}^+_{xy} = 0, \quad (22)$$

$$\mathcal{H}^+_{yy} = 2(-\gamma_x+\gamma_y). \quad (23)$$

For $\gamma_y>\gamma_x$ this critical point is a minimum, meanwhile for $\gamma_y<\gamma_x$ it is a saddle point.

(iii) $(x_c,y_c)=(0,\pm\sqrt{1-1/\gamma_y^2})$ and $\gamma_y<-1$: Now the elements of the Hessian matrix are

$$\mathcal{H}^+_{xx} = 2(\gamma_x-\gamma_y), \quad (24)$$

$$\mathcal{H}^+_{xy} = 0, \quad (25)$$

$$\mathcal{H}^+_{yy} = 2\gamma_y(1-\gamma_y^2) > 0. \quad (26)$$

Then we see that in the region $\gamma_x>\gamma_y$ the critical point is a minimum and in the region $\gamma_x<\gamma_y$, the critical point is a saddle point. Although these are similar to the previous conditions, we must observe that in this case $\gamma_y<-1$, whereas before the region was $\gamma_x<-1$.

(iv) (x_c,y_c) such that $x_c^2+y_c^2=1-1/\gamma_0^2$ and $\gamma_0\equiv\gamma_x=\gamma_y<-1$: In this final case, the elements of the Hessian matrix are

$$\mathcal{H}^+_{xx} = -2\gamma^3x_c^2 > 0, \quad (27)$$

$$\mathcal{H}^+_{xy} = 2\gamma^3x_cy_c, \quad (28)$$

$$\mathcal{H}^+_{yy} = -2\gamma^3y_c^2 > 0. \quad (29)$$

The determinant of the Hessian function is always zero. In this case our criterion says nothing about the nature of the critical point, but an expansion in spherical coordinates reveals that the energy surface is φ independent and a minimum at this locus of points.

For the lower hemisphere case—i.e., $\mathcal{E}^-$—we observe that if we make a parameter axis reflection

$$\gamma_x \to -\gamma_x,\ \gamma_y \to -\gamma_y,$$

then $\mathcal{E}^- \to -\mathcal{E}^+$. Therefore the analysis we made for $\mathcal{E}^+$ will be identical for $\mathcal{E}^-$ if we add to the above transformation the change of minimum for maximum, and maximum for minimum. In Table II of the Appendix the nature of the critical points associated to the function $\mathcal{E}^-$ is indicated.

A summary of the behavior of the critical points for the function $\mathcal{E}(\theta,\phi)$, in terms of points on the sphere (θ,ϕ), is presented in Table I.

The standard energy surface, in the region $\gamma_x \geq 1, \gamma_y \geq 1$, presents two minima, with the lowest one corresponding to the constant value $\mathcal{E}^+ = -2$.

For the other critical points, as can be seen in Tables II and III of the Appendix, only the function $\mathcal{E}^+$ presents minima and they all have the same functional form

$$\mathcal{E}^+(x_c,y_c) = \Gamma + \frac{1}{\Gamma}, \tag{30}$$

where we have defined

$$\Gamma = \begin{cases} \gamma_x, & \text{when } \gamma_x < -1, \quad \gamma_x < \gamma_y, \\ \gamma_y, & \text{when } \gamma_y < -1 \quad \gamma_y < \gamma_x, \\ \bar{\gamma}, & \text{when } \gamma_x = \gamma_y = \bar{\gamma}, \quad \bar{\gamma} < -1. \end{cases} \tag{31}$$

The study of the even and odd energy surfaces and their critical points cannot be performed analytically. These surfaces were built finding numerically their minima. As a reference, those minima at the critical points of the standard energy surface listed above are given. For the north and south poles, which correspond to $(x_c,y_c)=(0,0)$, the expressions are

$$\mathcal{E}_e = \pm 2,\ \mathcal{E}_o = \pm 2 + \frac{1}{j}(\gamma_x + \gamma_y \mp 2), \tag{32}$$

where for the up sign there is the condition $\gamma_x > -1$ and $\gamma_y > -1$, while for the down sign one has that $\gamma_x > 1$ and $\gamma_y > 1$.

In the other critical points, one can write the following expression for the even and odd energy surfaces:

$$\mathcal{E}_{e/o} = \left(\Gamma + \frac{1}{\Gamma}\right)\frac{\Gamma^{2j} \pm \Gamma^2}{\Gamma^{2j} \pm 1} \mp (\gamma_x + \gamma_y)\frac{\Gamma^2 - 1}{\Gamma^{2j} \pm 1}, \tag{33}$$

where $(x_c,y_c) \neq (0,0)$ and the parameter Γ satisfies the same conditions established in Eq. (31).

Thouless' theorem[22] allows a direct association of the Hartree-Fock trial ground state to the normal energy surfaces. Then, it is only necessary to multiply by the magnification and to add the shift to obtain the Hartree-Fock solution of the LMG Hamiltonian. In this sense, the even and odd coherent states can be understood as parity-projected Hartree-Fock states, which provide a good approximation for the ground and first-excited states of the system.

In a similar form other observables, like the distribution function of Dicke states, the expectation value of the number of particles in the upper level and its fluctuations are determined. The results at the minima critical points of these observables are compared with the corresponding quantum expressions in Sec. IV.

C. Phase transitions

A critical point belongs to a Maxwell set when the classical energies at two or more critical points are equal and under small changes of the control parameters satisfy the Clausius-Clapeyron equations.[15] When, while smoothly changing the control parameters, a Maxwell set is crossed, the energy surface jumps from one critical branch to another and a phase transition can take place. From the previous analysis it follows that a phase transition for the minima of the classical energy surface can only happen for $\Gamma \leq -1$.

The Maxwell sets must satisfy the Clausius-Clapeyron condition

$$\mathcal{E}^{(p)} = \mathcal{E}^{(q)},\ \{\partial\mathcal{E}^{(p)}/\partial\gamma_k - \partial\mathcal{E}^{(q)}/\partial\gamma_k\}\delta\gamma_k = 0, \tag{34}$$

with p and q running over the different critical points; the notation $(\gamma_1,\gamma_2)=(\gamma_x,\gamma_y)$ was used for the control parameters.

Bifurcation sets are the loci in parameter space where function ε changes because equilibria points are either created or destroyed. According to the previous discussion, the bifurcation sets are given by

$$\gamma_x = \pm 1, \quad \gamma_y = \pm 1, \quad \gamma_x = \gamma_y \ \text{ with } |\gamma_x| \geq 1. \tag{35}$$

The order of the phase transitions can be determined following the Ehrenfest classification of the classical phase transitions. A phase transition takes place between p and q branches of critical points and is of nth order if

$$\lim_{\delta\to 0} \left.\frac{\partial^i \mathcal{E}^{(p)}(s)}{\partial s^i}\right|_{s_0-\delta} = \lim_{\delta\to 0} \left.\frac{\partial^i \mathcal{E}^{(q)}(s)}{\partial s^i}\right|_{s_0+\delta}, \tag{36}$$

for $i=0,1,2,\ldots,n-1$, but fails for $i=n$.[15]

As an example, let us consider the function $\mathcal{E}^+(x,y)$ when the line $\gamma_x=-1$ is crossed along the straight lines $\gamma_y=\pm 2$, shown with arrow number 1 in Fig. 1. The control parameters γ_x and γ_y are described by the parametric equations

$$\gamma_x = -1 + \delta, \quad \gamma_y = 2. \tag{37}$$

The standard energy surface $\mathcal{E}^+$ evaluated at the critical points $(0,0)$ and $(x_c,0)$ is

$$\mathcal{E}^+(0,0) = -2, \quad \mathcal{E}^+(x_c,0) = \frac{1}{-1+\delta} - 1 + \delta, \tag{38}$$

respectively. To apply the Ehrenfest definition of a phase transition we calculate

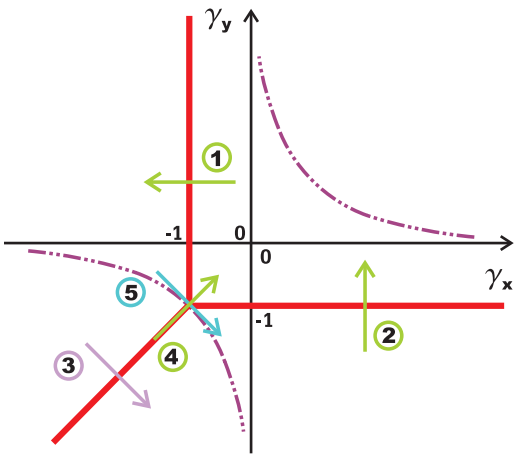

FIG. 1. (Color online) The bifurcation sets associated with the absolute minima of the standard energy surface are indicated by thick solid lines. The equilateral hyperbolas are also shown with dash-dotted lines. The arrows numerated from 1 to 5 are indicating phase transitions between the critical points associated with minima of the standard energy surface $\mathcal{E}^+$ given in Table II of the Appendix.

$$\mathcal{E}^+|_{(0,0),(-1+\delta,2)} = \mathcal{E}^+|_{(x_c,0),(-1+\delta,2)},$$

$$\left.\frac{\partial \mathcal{E}^+}{\partial \gamma_x}\right|_{(0,0),(-1+\delta,2)} = \left.\frac{\partial \mathcal{E}^+}{\partial \gamma_x}\right|_{(x_c,0),(-1+\delta,2)},$$

$$\left.\frac{\partial^2 \mathcal{E}^+}{\partial \gamma_x^2}\right|_{(0,0),(-1+\delta,2)} \neq \left.\frac{\partial^2 E^+}{\partial \gamma_x^2}\right|_{(x_c,0),(-1+\delta,2)},$$

where the different expressions are evaluated at the critical points $(x_c=0, y_c=0)$ and $(x_c \neq 0, y_c=0)$ and the control parameters $(\gamma_x=-1+\delta, \gamma_y=2)$ when $\delta \to 0$. Then, crossing the curve $\gamma_x=-1$, one finds a second-order transition of the Ginzburg-Landau type. In general a second-order phase transition takes place when the straight lines $\gamma_x=-1$ (arrow 1) and $\gamma_y=-1$ (arrow 2) and the point $(\gamma_x, \gamma_y)=(-1,-1)$ (arrow 4) are crossed. The crossing of the straight line $\gamma_y=\gamma_x$ (arrow 3) yields a first-order transition. Special attention must be given to the crossing of the point $(\gamma_x, \gamma_y)=(-1,-1)$ along the straight line $\gamma_y=-\gamma_x-2$ because in that case there is a third-order phase transition (arrow 5). In that point, a convergence of second-order phase transitions is taking place.

In Fig. 1 the bifurcation sets associated with phase transitions between minima are shown with thick lines. Those associated with maxima can be obtained by means of a reflection along the horizontal line $\gamma_x+\gamma_y=0$. Notice that there are second-order phase transitions when the minima of the system jumps from the critical points $(0,0) \to (x_c,0)$, $(0,y_c) \to (0,0)$, and $(x_c,y_c) \to (0,0)$ while the case $(x_c,0) \to (0,y_c)$ is first order. When one is crossing the point $(\gamma_x=-1, \gamma_y=-1)$, in the control parameter space, along the line $\gamma_y=-\gamma_x-2$ there is a third-order phase transition.

It is also shown that the parameter space is divided into three regions by the equilateral hyperbola

$$\gamma_y = \frac{1}{\gamma_x}, \tag{39}$$

which is obtained by equating the even and odd energy surfaces at the critical points that yield absolute minima. This function has consequences in the determination of the regions in the parameter space where there are crossings and anticrossings. On the upper branch of the equilateral hyperbolas there are crossings between the maximum even and odd energy surfaces while in the lower part one finds a similar behavior for the minima of these two energy surfaces. In between there are no crossings.

D. Dynamical behavior

The time-dependent variational principle is a formulation of the Schrödinger equation through a variation of an action functional. This formalism yields first-order equations of motion, which may be interpreted as Hamilton equations of motion, if certain conditions are satisfied by the overlap between the used parametrized states in the variational principle.[27] This formalism is closely related to the Feynman's path integral representation of quantum mechanics.[28]

Next we briefly review the symplectic structure for the LMG model. The classical equations of motion associated with our quantum Hamiltonian are built from the overlap of the non-normalized normal coherent states—i.e.,

$$\mathcal{N}(\zeta,\zeta^*) = \{\zeta|\zeta\} = (1+|\zeta|^2)^{2j}, \tag{40}$$

which allows the definition of the complex auxiliary function

$$\mathcal{C}(\zeta,\zeta^*) = \frac{\partial^2 \ln \mathcal{N}}{\partial \zeta\, \partial\, \zeta^*} = \frac{2j}{(1+\zeta\zeta^*)^2}. \tag{41}$$

This function is necessary to introduce the generalized Poisson brackets for arbitrary complex functions $A(\zeta,\zeta^*)$ and $B(\zeta,\zeta^*)$, given by[27,28]

$$\{A,B\} = \frac{i}{\mathcal{C}}\left\{\frac{\partial A}{\partial \zeta}\frac{\partial B}{\partial \zeta^*} - \frac{\partial A}{\partial \zeta^*}\frac{\partial B}{\partial \zeta}\right\}. \tag{42}$$

In this way, the classical equations of motion of the complex variables ζ, ζ^* are

$$\dot{\zeta} = \{\zeta, \mathcal{H}\}, \quad \dot{\zeta}^* = \{\zeta^*, \mathcal{H}\}, \tag{43}$$

where $\mathcal{H}=E(\theta,\phi)=E(\zeta,\zeta^*)$, given in Eq. (9). In summary, the overlap $\mathcal{N}(\zeta,\zeta^*)$ determines the kinematical aspects of the motion while $\mathcal{H}$ is responsible of the dynamics.

E. Trajectories

In terms of the angles θ and ϕ on the sphere, the generalized Poisson brackets take the form

$$\{A,B\} = -\frac{1}{j \sin\theta}\left\{\frac{\partial A}{\partial \theta}\frac{\partial B}{\partial \phi} - \frac{\partial A}{\partial \phi}\frac{\partial B}{\partial \theta}\right\}. \tag{44}$$

The Hamilton equations of motion

$$\dot{\theta} = \{\theta, \mathcal{H}\}, \quad \dot{\phi} = \{\phi, \mathcal{H}\}, \tag{45}$$

give rise to

$$\frac{\partial \theta}{\partial \tau} = (\gamma_x - \gamma_y)\sin\theta \sin(2\phi),$$

$$\frac{\partial \phi}{\partial \tau} = 2 + \cos\theta[\gamma_x + \gamma_y + (\gamma_x - \gamma_y)\cos(2\phi)], \tag{46}$$

where we have introduced $\tau = \omega t$.

To study this dynamical system (46) it is convenient to use the classical functions

$$j_x = \left\langle \zeta \middle| \frac{1}{2}(J_+ + J_-) \middle| \zeta \right\rangle = j \sin\theta \cos\phi,$$

$$j_y = \left\langle \zeta \middle| \frac{1}{2i}(J_+ - J_-) \middle| \zeta \right\rangle = j \sin\theta \sin\phi,$$

$$j_z = \langle \zeta | J_0 | \zeta \rangle = -j \cos\theta, \tag{47}$$

which satisfy the Poisson bracket relations for the angular momentum components. These classical functions obey the equations of motion

$$\frac{dj_x}{d\tau} = -2\left(1 - \frac{\gamma_y}{j} j_z\right) j_y, \quad \frac{dj_y}{d\tau} = 2\left(1 - \frac{\gamma_x}{j} j_z\right) j_x,$$

$$\frac{dj_z}{d\tau} = \frac{2}{j}(\gamma_x - \gamma_y) j_x j_y, \tag{48}$$

which are equivalent to the system (46)—i.e., describe the same motion over the sphere.

The case $\gamma_x = \gamma_y$ is straightforward and the solution is given by

$$j_z(\tau) = j_z(0), \quad j_x(\tau) = j_x(0)\cos\omega_0\tau - \sigma j_y(0)\sin\omega_0\tau,$$

$$j_y(\tau) = \sigma j_x(0)\sin\omega_0\tau + j_y(0)\cos\omega_0\tau, \tag{49}$$

where we have defined $\sigma = \mathrm{sgn}[1 - (\gamma_x/j) j_z(0)]$ and $\omega_0 = 2|1 - (\gamma_x/j) j_z(0)|$.

For $\gamma_x \neq \gamma_y$, the solutions are not analytical and the system of equations is solved numerically. According to the separatrix of the system, the phase transition regions in the parameter strength space are indicated in Fig. 1, through the arrows numerated from 1 to 5. In what follows, we present their classical energy surfaces and classical trajectories over the unitary sphere. Each figure displays the results for three sets of Hamiltonian parameters associated with each arrow plotted in Fig. 1. The upper panel was calculated at the beginning of the arrow, the middle panel at the phase transition, and the lower panel at the end of the arrow. The initial conditions j_{x0}, j_{y0}, and j_{z0} are selected over the unitary sphere with an energy 0.4 higher that the associated minimum energy.

In Fig. 2 we study the behavior of the standard energy surface and trajectories around the minimum of a second-order Ginzburg-Landau phase transition along arrow No. 1 in Fig. 1. A spherical minimum in the south pole is converted into two deformed minima along the j_x axis (only half the surface is shown) through a quartic potential on the bifurcation. The classical trajectories evolve around the minimum. In the bottom figure the initial conditions were selected to allow only the trajectory around one minimum; changing j_{x0} by $-j_{x0}$ gives a trajectory around the other minimum.

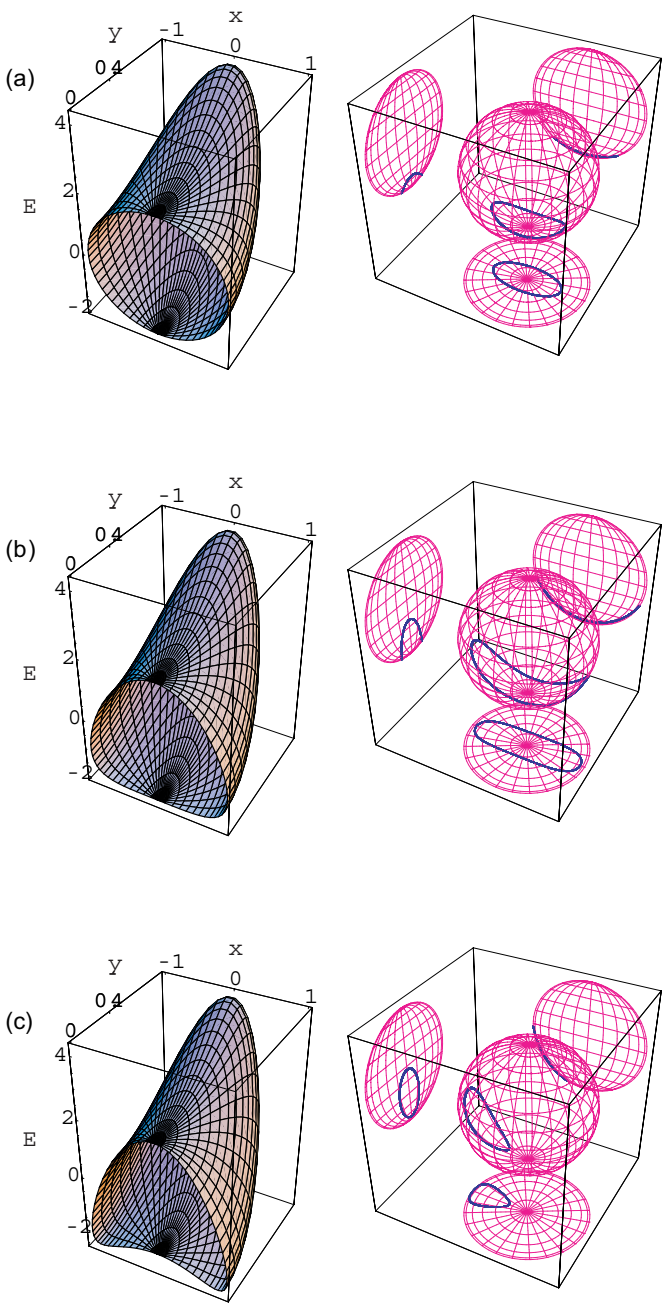

FIG. 2. (Color online) Energy surfaces (10) (left) and classical trajectories (right) for the functions j_x, j_y, and j_z with $j=1$. The parameter strengths, energy, and initial condition values are for (a) $(\gamma_x, \gamma_y) = (0,4)$, $\mathcal{E} = -1.6$, $(j_{x0}, j_{y0}, j_{z0}) = (0.01, 0.28, -0.96)$; (b) $(\gamma_x, \gamma_y) = (-1,4)$, $\mathcal{E} = -1.6$, $(j_{x0}, j_{y0}, j_{z0}) = (0.01, 0.28, -0.96)$; (c) $(\gamma_x, \gamma_y) = (-2,4)$, $\mathcal{E} = -2.1$, $(j_{x0}, j_{y0}, j_{z0}) = (-0.47, 0.14, -0.87)$.

In Fig. 3 the contour energy curves are shown, as a function of the variables (θ, ϕ), along this phase transition (arrow No. 1 in Fig. 1). In Figs. 3(a) and 3(b) the Hamiltonian parameters are the same employed in Figs. 2(a) and 2(c),

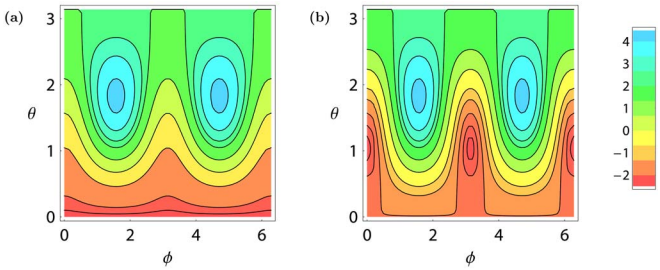

FIG. 3. (Color online) Contour plots of the energy surface (10): in (a) the parameters $\gamma_x=0$ and $\gamma_y=4$ are taken for the set of energies $-1.99,-1.9,-1.0,0,1.0,2.0,2.5,3.2,4.0$; while in (b) the parameters are $\gamma_x=-2$ and $\gamma_y=4$ and the energies $-2.45,-2.3,-2.0,-1.5,-1.0,0,1.0,2.0,2.5,3.2,4.0$.

respectively. In the first case the five lowest lines depict the classical trajectories for energies $E=-1.99,-1.9,-1.0,0,1.0$, which represent rotational motions with the angle ϕ unbounded. At the energy $E=2.0$ the saddle point $\theta_c=\pi$ is reached. For higher energies, the trajectories are in the libration regime, where both angles θ and ϕ have lower and upper bounds, associated with displacements inside the "horn" in Fig. 2(a). At the point $(\gamma_x=-1,\gamma_y=4)$, the energy surface is characterized by a quartic function, which is very soft with respect to the motion in θ. In Fig. 3(b) the motion is rotational for $|E|>2$, where it reaches the saddle point $\theta_c=0$, and of the libration type for $-2<E<2$.

These sudden changes in the trajectories represent phase transitions, as a function of the energy of the system, for fixed values of the Hamiltonian parameters. The energies where they occur are sometimes called the "energy separatrix,"[4] which should not be confused with the separatrix in the parameter space depicted in Fig. 1, associated with phase transitions which take place in the ground state when the Hamiltonian parameters are varied.

The phase transition along arrow No. 2 in Fig. 1 is also a second-order transition of the Ginzburg-Landau type, similar than the previous one. In this case the energy surface presents two minima with equal depths in direction of the j_y axis and changes to a spherical potential, again through a quartic potential, at the bifurcation. The associated contour energy plots are similar to those exhibited in Fig. 3, but viewed from right to left. They display a phase transition from a deformed case, with two saddle point bifurcations separating the libration from the rotational motions, to a spherical one, with one saddle point bifurcation.

In Fig. 4 we study the behavior of the standard energy surface and trajectories around the minimum, for the first-order transition along arrow No. 3 in Fig. 1. Two deformed minima along the j_x axis evolve in two deformed minima along the j_y axis through a ϕ-unstable potential on the bifurcation. In the top figure the initial conditions were selected again to allow only the trajectory around the left minimum; changing j_{x0} by $-j_{x0}$ gives a trajectory around the right minimum. Something similar happens with the trajectory shown in the bottom figure.

For this case, the contour energy plots are shown in Fig. 5. In Fig. 5(a), the closed trajectories associated with libration motions are clearly seen around the minima

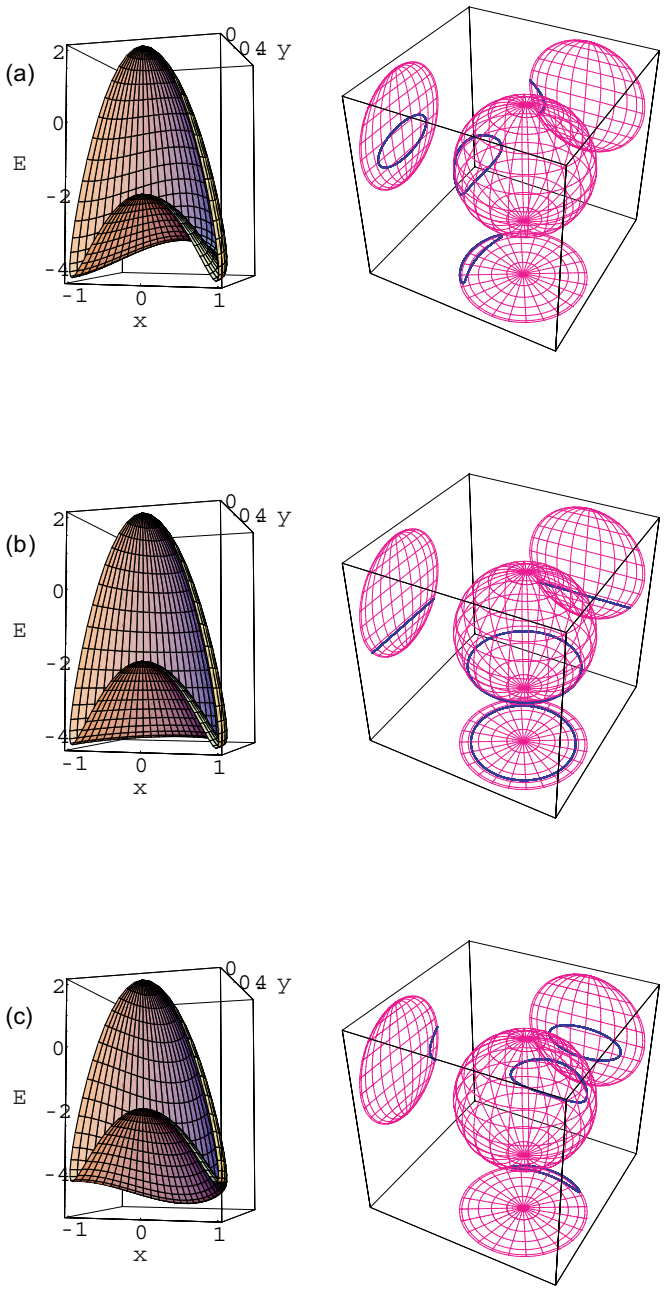

FIG. 4. (Color online) The same as in Fig. 2 for (a) $(\gamma_x,\gamma_y)=(-4,-3)$, $\mathcal{E}=-3.85$, $(j_{x0},j_{y0},j_{z0})=(-0.96,0.28,0.03)$; (b) $(\gamma_x,\gamma_y)=(-4,-4)$, $\mathcal{E}=-3.85$, $(j_{x0},j_{y0},j_{z0})=(0.01,0.82,-0.57)$; (c) $(\gamma_x,\gamma_y)=(-4,-5)$, $\mathcal{E}=-4.8$, $(j_{x0},j_{y0},j_{z0})=(0.4,0.82,-0.42)$.

$(\theta_c=1.318,\phi_c=0)$ and $(\theta_c=1.318,\phi_c=\pi)$ (central regions). At the energy $E=-10/3$, the saddle points on the energy surface, $(\theta_c=1.231,\pi/2)$ and $(\theta_c=1.231,3\pi/2)$, are reached. For $-10/3<E<-2$, there are always two possible rotational trajectories, over the inner and outer surfaces in Fig. 4(a), for the two values of θ, until a new bifurcation with an energy $E=-2.0$ is reached. For higher energies only one rotational trajectory—i.e., one value of θ—is allowed for each energy. In Fig. 5(b), one finds only a rotational motion, again for two values of θ, until the energy of the previous bifurcation set is obtained. Figure 5(c) is similar to Fig. 5(a), but now the

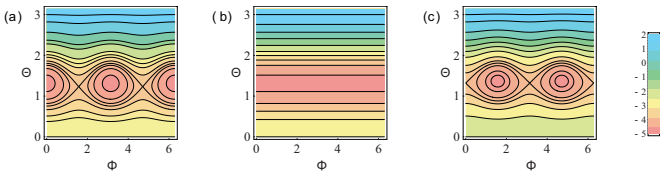

FIG. 5. (Color online) Contour plots of the energy surface (10): in (a), one considers $\gamma_x=-4$ and $\gamma_y=-3$; with the set of energies $\{-4.1,-3.75,-3.5,-10/3,-3.1,-2.7,-2.4,-2.0,-1.0,-0.5, 0.5,1.5,1.9\}$; in (b) one has $\gamma_x=-4$ and $\gamma_y=-4$ with energies $\{-4.1,-3.0,-2.5,-2.0,-1.2,-0.3,0.5,1.3,1.9\}$; and in (c) the parameters are $\gamma_x=-4$ and $\gamma_y=-5$ and the energies $\{-5.1,-4.9, -4.5,-17/4,-4.0,-3.5,-2.7,-2.0,-1.3,-0.5, 0.5,1.5,1.9\}$.

libration motions for $E<-17/4$ take place around $(\theta_c=1.369,\phi_c=\pi/2)$ or $(\theta_c=1.369,\phi_c=3\pi/2)$.

It is worth mentioning that energy phase transitions, as seen in the trajectories by increasing the energy through saddle points, can occur between libration and rotational motion or from a kind of rotational motion with two allowed trajectories to another one with only one possible trajectory.

In Fig. 6 it is shown a second-order transition from a ϕ-unstable potential to a spherical minimum along arrow No. 4 in Fig. 1. The three trajectories are horizontal—i.e., have constant j_z. In this particular case they can be found analytically. The contour energy plots in this case correspond always to a rotational motion, with saddle point bifurcations separating the cases when the motion can have two values of θ from the rotational motion where there is only one value of θ.

In Fig. 7 we observe a behavior similar to the one shown in Fig. 4, although the transition in this case is of third order along arrow No. 5 in Fig. 1.

For this case, the contour energy plots are shown in Fig. 8. In Fig. 8(a), the closed trajectories associated with libration motions are seen around the minima $(\theta_c=1.047,\phi_c=0)$ and $(\theta_c=1.047,\phi_c=\pi)$ (central regions). At higher energies, the system exhibits rotational motion. In this case for the same energy, rotational motions are present with only one possible value of θ. In Fig. 8(b), only rotational motion is present. In Fig. 8(c), the energy minima are located at $(\theta_c=1.047,\phi_c=\pi/2)$ and $(\theta_c=1.047,\phi_c=3\pi/2)$. Thus there are phase transitions from libration motions to rotational motions besides for a change of the minima of the energy surface. There is again a phase transition from libration to rotational motions at $E=-2$.

It is relevant to characterize the classical solution of the LMG model. The power spectrum[29] of the classical trajectories $(j_x(t),j_y(t),j_z(t))$ indicates that the motion is periodic. Depending on the values of the control parameters γ_x and γ_y, the number of frequencies runs from 1, when $\gamma_x=\gamma_y$, to a finite number of them otherwise. For $\gamma_x\neq\gamma_y$ we note that increasing the value of the energy, the number of participant frequencies grows. The evaluation of the Lyapunov exponents confirms that the motion is periodic. This is of course consistent with the quantum analysis, because the system is integrable, having three degrees of freedom and three constants of motion: the number of particles, N; the square of the total angular momentum, $\hat{J}^2$; and the energy E.

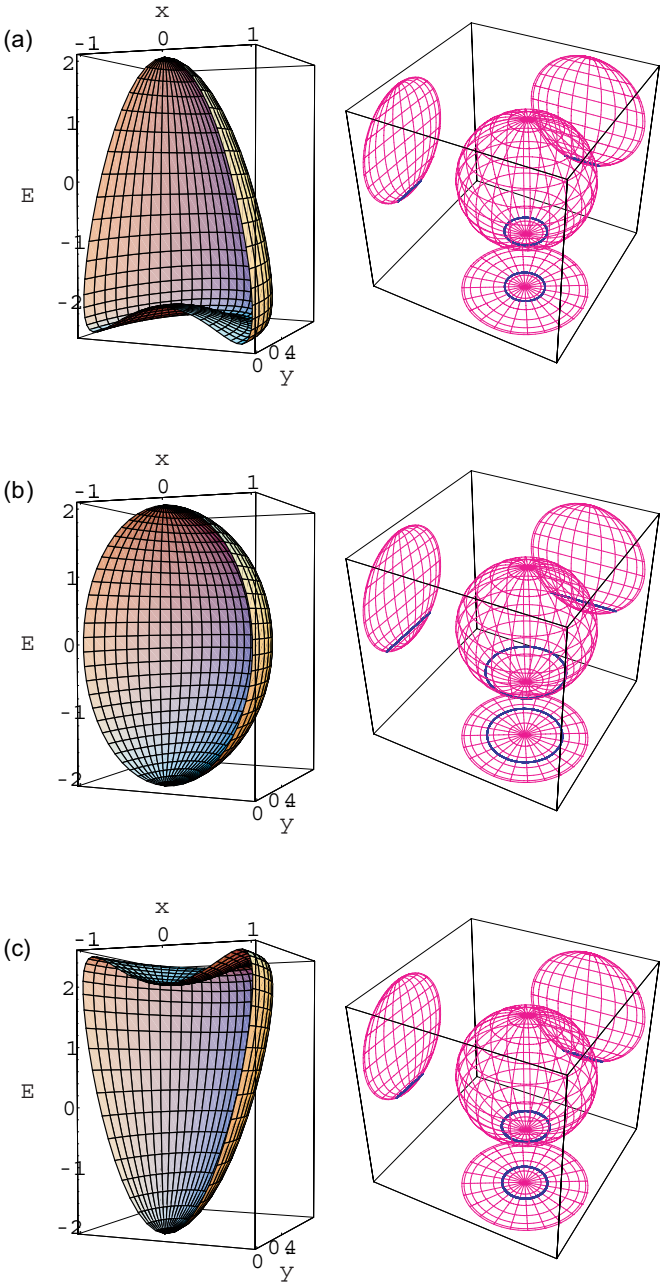

FIG. 6. (Color online) The same as in Fig. 2 for (a) $(\gamma_x,\gamma_y)=(-2,-2)$, $\mathcal{E}=-2.1$, $(j_{x0},j_{y0},j_{z0})=(0.01,0.32,-0.95)$; (b) $(\gamma_x,\gamma_y)=(0,0)$, $\mathcal{E}=-1.6$, $(j_{x0},j_{y0},j_{z0})=(0.01,0.60,-0.80)$; (c) $(\gamma_x,\gamma_y)=(2,2)$, $\mathcal{E}=-1.6$, $(j_{x0},j_{y0},j_{z0})=(0.01,0.36,-0.93)$.

IV. COMPARISON OF QUANTUM AND CLASSICAL ANALYSIS

In order to compare the trial coherent-state description and the exact quantum solutions, one considers the following form of the Hamiltonian:

$$H=\frac{j(\gamma_x+\gamma_y)}{2j-1}+\frac{2}{j}J_0-\frac{(\gamma_x+\gamma_y)}{j(2j-1)}J_0^2+\frac{(\gamma_x-\gamma_y)}{2j(2j-1)}(J_+^2+J_-^2),$$

which has the same shift and scaling that were used in the classical analysis.

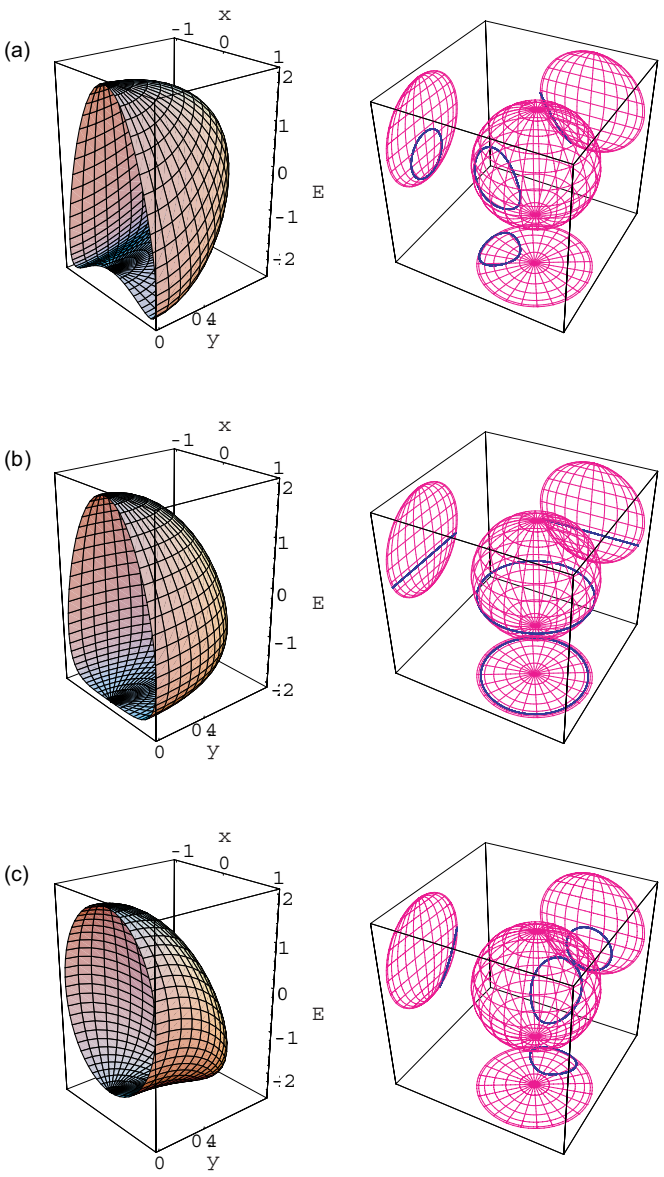

FIG. 7. (Color online) The same as in Fig. 2 for (a) $(\gamma_x,\gamma_y)=(-2,0)$, $\mathcal{E}=-2.1$, $(j_{x0},j_{y0},j_{z0})=(-0.86,0.41,-0.32)$; (b) $(\gamma_x,\gamma_y)=(-1,-1)$, $\mathcal{E}=-1.6$, $(j_{x0},j_{y0},j_{z0})=(0.01,0.93,-0.38)$; (c) $(\gamma_x,\gamma_y)=(0,-2)$, $\mathcal{E}=-2.1$, $(j_{x0},j_{y0},j_{z0})=(-0.07,0.33,-0.94)$.

It has been shown that the classical dynamics of the system depends on the regions on the parameter space classified by the separatrix of the Hamiltonian model. This is evident in the energy surfaces, their phase transitions, and the available trajectories on the sphere. If the initial conditions are properly selected—i.e., very close to the locus of points that define the separatrix—the system evolves around stable or unstable equilibrium points, spending more time when its trajectory is closer to them.

The behavior of the quantum system can also be described in terms of the separatrix of the model. It can be seen in the manifolds of the ground and first excited energies, presented in Ref. 20. The bifurcation sets $\gamma_x=-1$, $\gamma_y=-1$ for values of $\gamma_x<-1$, $\gamma_y<-1$ and the cusp[15] found in the classical analysis closely describe the sudden changes in the

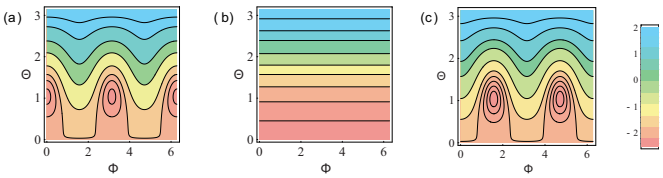

FIG. 8. (Color online) Contour plots of the energy surface (10): in (a) one uses $\gamma_x=-2$ and $\gamma_y=0$ with the energies $-2.45,-2.25,-2.0,-1.5,-1.0,-0.5,0.5,1.5,1.99$. In (b) the parameters are $\gamma_x=-1$ and $\gamma_y=-1$ with the contours $-1.99,-1.85,-1.5,-1.0,-0.5,0.2,1.0,1.5,1.9$. In part (c), $\gamma_x=0$ and $\gamma_y=-2$ with the curves $-2.45,-2.35,-2.2,-2.0,-1.7,-1.0,-0.5,0.0,0.7,1.5,1.9$.

slopes seen in these plots. The exact even and odd minimum energies cross at the same hyperbola, defined in Eq. (39), as the even and odd energy surfaces do. This is clearly shown in Ref. 20, which underlines the strong correspondence between the classical and quantum descriptions of the system.

To study the behavior of the exact even and odd eigenfunctions of the LMG model in the vicinity of the bifurcation and Maxwell sets all along the phase transitions, we compare the composition of Dicke states of the eigensolution with those associated to the minima for the standard, even, and odd coherent states.

In the case of the phase transition indicated by the arrows with a number 1 in Fig. 1, there is a second-order phase transition between a spherical energy surface to a deformed energy surface in the direction j_x. This transition is reflected in the composition of the exact wave function of the system which is dominated in the region with $\gamma_x>-1$ almost for a single Dicke state, while for $\gamma_x<-1$ the exact wave function includes the participation of many Dicke states.

In Figs. 9(a) and 9(b), the overlap between the even spin coherent state and the exact eigenfunctions of the ground

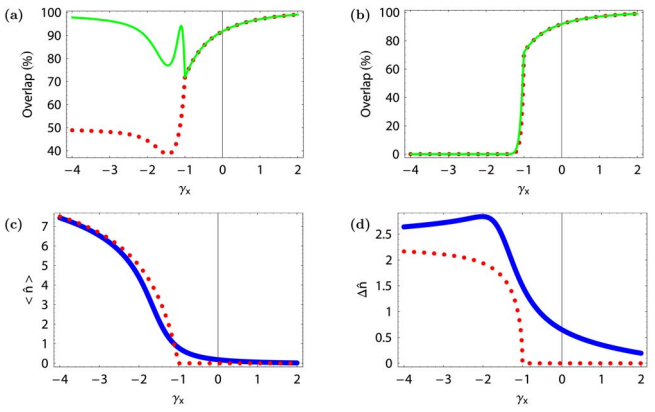

FIG. 9. (Color online) The overlaps between the even eigenfunctions of the LMG Hamiltonian with the even and standard spin coherent states are shown with solid and dotted lines, respectively. The expectation values of the population operator $\hat{n}$ and its corresponding fluctuation $\Delta\hat{n}$ with respect to the even exact solution and the standard spin coherent states are displayed with solid and dotted lines, respectively. In (a) and (c) the parameters of the trial states take the values $\phi_c=0$ or π and $z_c=-1/\gamma_x$, while in (b) and (d) correspond to a single Dicke state with $n=0$. We use $N=20$ and $\gamma_y=4$.

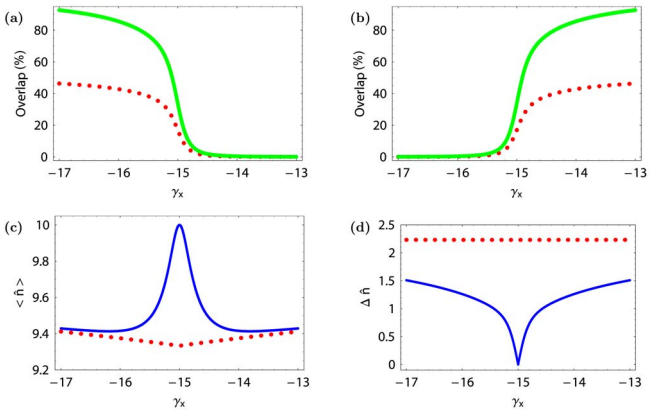

FIG. 10. (Color online) The overlaps between the even eigenfunctions of the LMG Hamiltonian with the even and standard spin coherent states are shown with solid and dotted lines, respectively. The expectation values of $\hat{n}$ and its corresponding fluctuation $\Delta\hat{n}$ with respect to the even exact eigenfunctions and standard spin coherent states are displayed with solid and dotted lines, respectively. In (a) and (c) the parameters are $\phi_c=0$ or π and $z_c=-1/\gamma_x$ while in (b) and (d) correspond to $\phi_c=\pi/2$ or $3\pi/2$ and $z_c=-1/\gamma_y$. We take $N=20$ and $\gamma_y=-\gamma_x-30$.

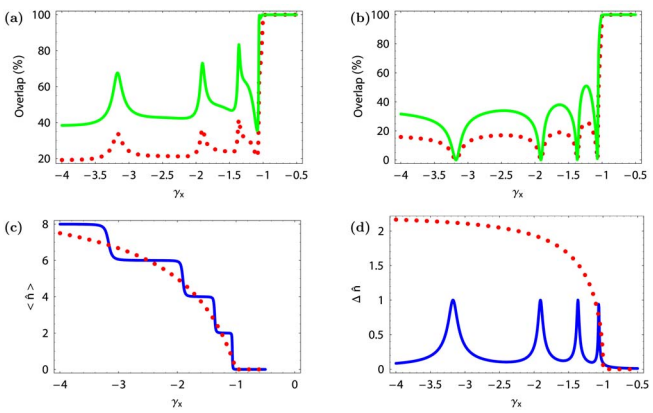

FIG. 11. (Color online) The overlaps between the even eigenfunctions of the LMG Hamiltonian with the even and standard spin coherent states are shown with solid and dotted lines, respectively. The expectation values of the population operator $\hat{n}$ and its corresponding fluctuation $\Delta\hat{n}$ with respect to the even exact eigenfunctions and standard spin coherent state are displayed with solid and dotted lines, respectively. In (a) and (c) the parameters are $\phi_c=0$ or π and $z_c=-1/\gamma_x$ while in (b) and (d) correspond to $\phi_c=\pi/2$ or $3\pi/2$ and $z_c=-1/\gamma_y$. We consider $N=20$ and $\gamma_y=\gamma_x+0.015$.

state of the model Hamiltonian is displayed with solid lines. The control parameters vary along the $\gamma_y=4$ straight line. For $\gamma_x<-1$ the dominant trial wave function is the even spin coherent state with the values $\phi_c=0$ or π and $z_c=-1/\gamma_x$, while for $\gamma_x>-1$ the dominant trial wave function is characterized by a single Dicke state, with $n=0$, as can be seen in the results of the expectation value of the population operator. The expectation values of the population operator, given in Fig. 9(c), and its corresponding fluctuation, given in Fig. 9(d), with respect to the ground-state solution, for $N=20$ particles, exhibit a smoothed phase transition. However, a change in the concavity of the curve can be appreciated in both calculations. The corresponding expressions for the standard spin coherent states show the phase transition at the bifurcation set $\gamma_x=-1$.

It is important to mention that the behavior along the bifurcation $\gamma_y=-1$, which is the phase transition indicated with the number 2 in Fig. 1, is very similar to the one discussed previously. In this case, there is a transition from a deformed energy surface in direction j_y to a spherical energy surface. Thus the composition of the exact wave functions is changing from many Dicke states to almost a single one. For this case the even spin coherent state with $\phi_c=\pi/2$ or $3\pi/2$ and $z_c=-1/\gamma_y$ is the best trial wave function in the region $\gamma_y<-1$ and $\gamma_x\geq 0$.

What happens for the previous phase transitions at the region $\gamma_x<0$ and $\gamma_y<0$? In this region there are many phase transitions in which the ground and first-excited states are described alternatively by the exact even and odd solutions. The first region of degeneracy starts at the equilateral hyperbola $\gamma_y=1/\gamma_x$. For a given number of particles, N, there are $N/2$ or $(N-1)/2$ values of the control parameter where there are degeneracy between the even and odd exact solutions, depending if the value of N is even or odd, respectively. Analytical expressions for the values of the control parameters (γ_x,γ_y) along the degeneracy lines were given in Ref. 20.

To study the phase transition along the bifurcation indicated by arrow No. 3 in Fig. 1, the overlap between the exact solution and the trial wave function calculated along the $\gamma_y=-\gamma_x-30$ straight line is presented in Fig. 10. The trial wave functions fail to reproduce the exact results in the vicinity of the bifurcations, as can be seen in the expectation value of the population, where the maximum disagreement happens at $\gamma_x=-15$—i.e., at the separatrix. Something similar occurs

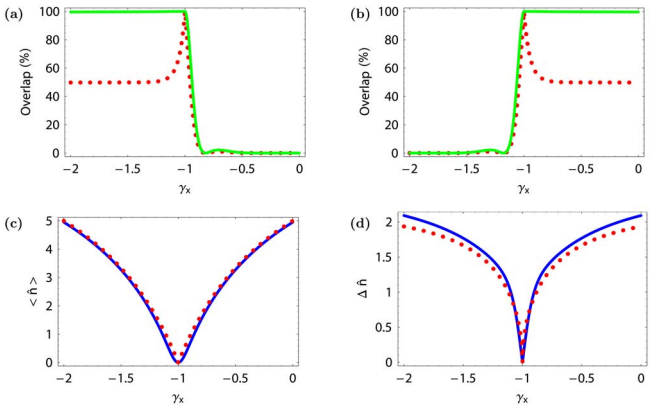

FIG. 12. (Color online) The overlaps between the even eigenfunctions of the LMG Hamiltonian with the even and standard spin coherent states are shown with solid and dotted lines, respectively. The expectation values of the population operator $\hat{n}$ and its corresponding fluctuation $\Delta\hat{n}$ with respect to the even exact solutions and standard spin coherent state are displayed with solid and dotted lines. In (a) and (c) the parameters take the values $\phi_c=0$ or π and $z_c=-1/\gamma_x$ while in (b) and (d) take $\phi_c=\pi/2$ or $3\pi/2$ and $z_c=-1/\gamma_y$. We use $N=20$ and $\gamma_y=-\gamma_x-2$.

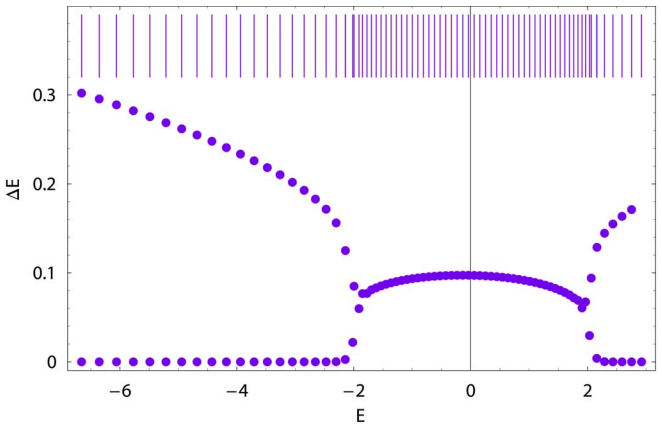

FIG. 13. (Color online) The distributions of nearest-neighbor spacings as a function of the energy is shown. In the upper part, the energy spectra is displayed, for the control parameters $(\gamma_x=2.5, \gamma_y=-6.5)$. There are two regions of degenerated energy levels and a zone of almost constant separation between the levels. In the plots, $N=100$ particles.

with the fluctuations of the population. In this case the even spin coherent state is the best trial wave function in all the considered region.

A similar result is obtained for the overlap between the exact odd eigenfunction and the odd spin coherent state. In some regions the ground state is best reproduced by the even spin coherent state and, in others, by the odd spin coherent state. These spin coherent states are constructed with the variable ϕ_c taking the values 0 or π and $z_c=-1/\gamma_x$ for $\gamma_y>\gamma_x$, while they are $\phi_c=\pi/2$ or $3\pi/2$ and $z_c=-1/\gamma_y$ for $\gamma_y<\gamma_x$. For $\gamma_y=\gamma_x$, the solution is diagonal in the Dicke basis and they are independent of ϕ.

The phase transition indicated by arrow No. 4 in Fig. 1 corresponds to a ϕ-unstable deformed energy surface to a spherical one. The composition of the exact wave functions is dominated for a single Dicke state, running from the value $n=j$ in the region $\gamma<-3.5$ to $n=0$ for $\gamma\geq-1$. To show that, the composition of the exact wave function, the expectation value of the number of particles, and its fluctuation are displayed in Fig. 11, along the straight line $\gamma_y=\gamma_x+0.015$. It can be noticed that the expectation value of the population operator changes suddenly at the values 2, 4, 6, and 8 but follows the result obtained with the standard coherent state. At each point where there is a phase transition, the overlap decreases considerably; this effect can be seen also in the calculation of the fluctuation of the population operator when it takes the value 1.

In Fig. 12, the overlaps of the quantum solutions and the trial wave functions, for the phase transition along the cusp of the system—i.e., $\gamma_y=-\gamma_x-2$—are displayed. In this case the even spin coherent state is the best trial wave function with the parameters $\phi_c=0$ or π and $z_c=-1/\gamma_x$ in the region $\gamma_x<-1$ and with $\phi_c=\pi/2$ or $\phi=3\pi/2$ and $z_c=-1/\gamma_y$ for $\gamma_x>-1$. The expectation value of the population operator is also shown, together with its corresponding fluctuation. They are both well reproduced by the trial wave function, except in a close neighborhood of the cusp point $(\gamma_x=-1, \gamma_y=-1)$.

It is interesting to study the distributions of nearest-neighbor spacings as a function of the number of eigenstate when the matrix Hamiltonian is not diagonal. The case $\gamma_y=-\gamma_x-4$ will be discussed, with $N=100$ particles. The behavior of the excitation energy spectra is also presented. In Fig. 13, for $(\gamma_x=2.5, \gamma_y=-6.5)$, the distribution function of spacings exhibits two regions of degenerated energy levels (zero spacings) intertwined with spacings varying between 0 and 0.3. In between there is a zone with almost constant separation between the energy levels with energies between −2 and 2. The degeneracies at the left-hand side of the distribution function correspond to the lower-energy region, including the ground state, while those appearing at the right-hand side belong to the higher excitation energy. The separation between the degenerate levels is richer and more complex than for the diagonal case. It is important to mention that the separatrix indicates exactly where the distribution function of spacings of the energy levels is not degenerated.

Finally, the expectation value of the population operator for $N=100$ is given in Fig. 14, where the control parameters are changing along the $\gamma_y=\gamma_x+0.015$ straight line in the interval $-4<\gamma_x<0$. The difference between the results associated with the exact even eigensolution with the odd case is the starting value—i.e., $\langle n\rangle=0$ in the even case while $\langle n\rangle=1$ for the odd one. For this large number of particles, one can see clearly the presence of the phase transition in the expectation value of the population operator and the excellent agreement with the trial wave functions. These results resemble the ones presented in Refs. 6 and 7, for the magnetization.

To summarize, if one is restricted to the region $\gamma_y>-1$ and $\gamma_x>-1$, the best trial wave function of the ground state of the system corresponds to the Dicke state with $n=0$, whereas that for the region $\gamma_x<-1$ and $\gamma_y>-1$ the even spin coherent state describes the ground state with parameters $\phi=0$ or π and $z=-1/\gamma_x$. For $\gamma_x>-1$ and $\gamma_y<-1$, one has that the best trial wave function is the even spin coherent state but now with $\phi_c=\pi/2$ or $3\pi/2$ and $z_c=-1/\gamma_y$. The most interesting region for a finite number of particles is when $\gamma_x<-1$ and $\gamma_y<-1$, because there are many phase transitions between the even and odd spin coherent states, as many

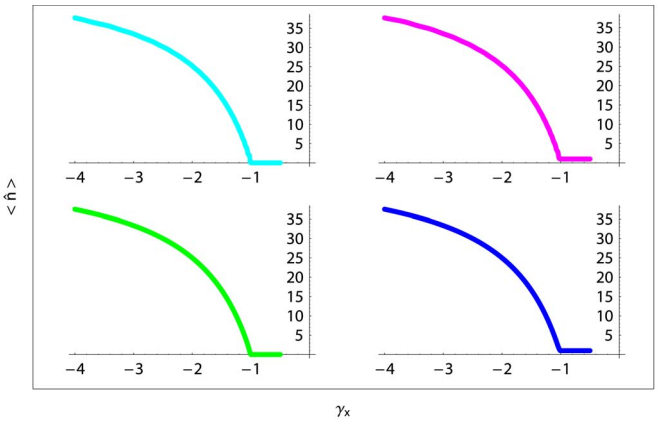

FIG. 14. (Color online) The expectation values of the population operator are shown for $N=100$ particles. In the first row, they correspond to the exact even and odd eigenfunctions, while in the second one to the even and odd spin coherent states, respectively. We take $\gamma_y=\gamma_x+0.015$ and $-4<\gamma_x<0$.

as half the considered number of particles. In this case the dominant even or odd spin coherent states take the values $\phi_c=0$ or π and $z_c=-1/\gamma_x$ if $\gamma_y>\gamma_x$ and the parameters are $\phi_c=\pi/2$ or $3\pi/2$ and $z_c=-1/\gamma_y$ if $\gamma_y<\gamma_x$.

V. CONCLUSIONS

The LMG model describes a spin system with nonlinear interactions. It displays a very rich behavior when the two-body interaction strengths are varied. The exact quantum solutions exhibit both crossings between levels with different parities and anticrossings (level repulsion) between states with the same parities. The exact energy surfaces show sudden changes in their slopes for certain parameter values, which were associated with classical phase transitions. Standard, even, and odd coherent states allowed the construction of the respective energy surfaces. For the standard energy surface, the catastrophe formalism allowed for a complete classification of the critical points. Some of them belong to the bifurcation and Maxwell sets and define the separatrix of the model. The separatrix is fundamental to describe the stability properties, phase transitions, and accidental degeneracies of the nonlinear spin Hamiltonian. The bifurcation sets displayed by the thick solid line in Fig. 1 separate the regions in the parameter space where single-particle motion dominates from those which are collective. For $\gamma_x<-1$ and $\gamma_y<-1$ the eigenstates have many components on the angular momentum basis states, while for the region $\gamma_x\geq-1$ and $\gamma_y\geq-1$, only one component is dominant. We found that according to the Clausius-Clapeyron classification there are first-, second-, and even third-order phase transitions for the LMG model, depending on how the parameters are changed to cross the separatrix. Even and odd energy surfaces were shown to closely reproduce the exact quantum behavior of the ground and first-excited states and their crossings, described by the hyperbola of Eq. (39). In the parameter region between the branches of the hyperbola there are no crossings between energy levels, whereas in the exterior part, degeneracy is present.

ACKNOWLEDGMENT

This work was partially supported by CONACyT, México, and by DGAPA-UNAM.

APPENDIX: CRITICAL POINTS

The critical points of the energy surface are evaluated by means of the equation $\nabla\mathcal{E}^{\pm}(x,y;\gamma_x,\gamma_y)=0$. For these functions one finds the derivatives

$$\frac{\partial\mathcal{E}^{\pm}}{\partial x}=2x\left(\gamma_x\pm\frac{1}{\sqrt{1-x^2-y^2}}\right), \tag{A1}$$

$$\frac{\partial\mathcal{E}^{\pm}}{\partial y}=2y\left(\gamma_y\pm\frac{1}{\sqrt{1-x^2-y^2}}\right). \tag{A2}$$

The functions $\mathcal{E}^{\pm}$ have several critical points, depending on the values of the parameters γ_x and γ_y as is indicated in Tables II and III.

TABLE II. The critical points of the function $\mathcal{E}^{+}$ are indicated in the first column. In the second column, it is established the region in the control parameter space where they are maximum, minimum, or saddle points.

(x_c,y_c)	Parameter region and character
$(0,0)$	$1+\gamma_x\geq0$, $1+\gamma_y\geq0$ } minimum
	$1+\gamma_x<0$, $1+\gamma_y<0$ } maximum
	$1+\gamma_x\geq0$, $1+\gamma_y\leq0$ } saddle
	$1+\gamma_x<0$, $1+\gamma_y>0$ } saddle
$(\pm\sqrt{1-1/\gamma_x^2},0)$	$\gamma_x<-1$ existence $\gamma_x>\gamma_y$ saddle $\gamma_x<\gamma_y$ minimum
$(0,\pm\sqrt{1-1/\gamma_y^2})$	$\gamma_y<-1$ existence $\gamma_x>\gamma_y$ minimum $\gamma_x<\gamma_y$ saddle
$x_c^2+y_c^2=1-1/\gamma_0^2$	$\gamma_0\equiv\gamma_x=\gamma_y<-1$ existence

The point $(0,0)$ is a critical point for any values of the parameters of the functions $\mathcal{E}^{\pm}(x,y)$. For this reason these particular values of γ_x and γ_y are called *the fundamental roots*.[15] The Taylor series expansion around these fundamental roots are

TABLE III. The same as in Table II but now for $\mathcal{E}^{-}$.

(x_c,y_c)	Parameter region and character
$(0,0)$	$1-\gamma_x\geq0$, $1-\gamma_y\geq0$ } maximum
	$1-\gamma_x<0$, $1-\gamma_y<0$ } minimum
	$1-\gamma_x\geq0$, $1-\gamma_y\leq0$ } saddle
	$1-\gamma_x<0$, $1-\gamma_y>0$ } saddle
$(\pm\sqrt{1-1/\gamma_x^2},0)$	$\gamma_x>1$ existence $\gamma_x<\gamma_y$ saddle $\gamma_x>\gamma_y$ maximum
$(0,\pm\sqrt{1-1/\gamma_y^2})$	$\gamma_y>1$ existence $\gamma_x<\gamma_y$ maximum $\gamma_x>\gamma_y$ saddle
$x_c^2+y_c^2=1-1/\gamma_0^2$	$\gamma_0\equiv\gamma_x=\gamma_y>1$ existence

$$\mathcal{E}^{\pm}(x,y) = \mp 2 + (\gamma_x \pm 1)x^2 + (\gamma_y \pm 1)y^2 \pm 6(x^4 + y^4) \pm 2x^2y^2 + O(5). \quad \text{(A3)}$$

Lower-order terms in this series, except for the constant one, can be eliminated by a proper choice of the control parameters γ_x and γ_y. We observe that the first term which cannot be canceled in this way is $\pm 6(x^4+y^4) \pm 2x^2y^2$, which characterizes a fourth-order germ of the system. From this germ, other critical points, different from the poles in the sphere, bifurcate as the control parameters are varied.

[1] A. S. Sorensen, L. M. Duan, J. I. Cirac, and P. Zoller, Nature (London) **409**, 63 (2001).
[2] M. Kitagawa and M. Ueda, Phys. Rev. A **47**, 5138 (1993).
[3] J. Vidal, G. Palacios, and C. Aslangul, Phys. Rev. A **70**, 062304 (2004); J. I. Latorre, R. Orus, E. Rico, and J. Vidal, *ibid.* **71**, 064101 (2005).
[4] A. Micheli, D. Jaksch, J. I. Cirac, and P. Zoller, Phys. Rev. A **67**, 013607 (2003).
[5] K. Molmer and A. Sorensen, Phys. Rev. Lett. **82**, 1835 (1999).
[6] R. Botet and R. Jullien, Phys. Rev. B **28**, 3955 (1983).
[7] W. D. Heiss, F. G. Scholtz, and H. B. Geyer, J. Phys. A **38**, 1843 (2005); F. Leyvraz and W. D. Heiss, Phys. Rev. Lett. **95**, 050402 (2005).
[8] S. Dusuel and J. Vidal, Phys. Rev. B **71**, 224420 (2005).
[9] J. N. Kriel, A. Y. Morozov, and F. G. Scholtz, J. Phys. A **38**, 205 (2005).
[10] A. Messikh, Z. Ficek, and M. R. B. Wahiddin, Phys. Rev. A **68**, 064301 (2003).
[11] J. N. Ginocchio and M. W. Kirson, Phys. Rev. Lett. **44**, 1744 (1980); A. E. L. Dieperink, O. Scholten, and F. Iachello, *ibid.* **44**, 1747 (1980).
[12] R. Gilmore, J. Math. Phys. **20**, 891 (1979); R. Gilmore, C. M. Bowden, and L. M. Narducci, Phys. Rev. A **12**, 1019 (1975).
[13] E. López-Moreno and O. Castaños, Rev. Mex. Fis. **42**, 163 (1996); Phys. Rev. C **54**, 2374 (1996).
[14] D. H. Feng, R. Gilmore, and S. R. Deans, Phys. Rev. C **23**, 1254 (1981).
[15] R. Gilmore, *Catastrophe Theory for Scientists and Engineers* (Wiley, New York, 1981).
[16] E. López-Moreno and O. Castaños, Rev. Mex. Fis. **44**, S48 (1998); J. E. García-Ramos, J. M. Arias, J. Barea, and A. Frank, Phys. Rev. C **68**, 024307 (2003).
[17] J. Jolie, P. Cejnar, R. F. Casten, S. Heinze, A. Linnemann, and V. Werner, Phys. Rev. Lett. **89**, 182502 (2002).
[18] F. Iachello, Phys. Rev. Lett. **85**, 3580 (2000); **87**, 052502 (2001).
[19] P. Cejnar, S. Heinze, and J. Jolie, Phys. Rev. C **68**, 034326 (2003).
[20] O. Castaños, R. López-Peña, J. G. Hirsch, and E. López-Moreno, Phys. Rev. B **72**, 012406 (2005).
[21] H. J. Lipkin, N. Meshkov, and A. J. Glick, Nucl. Phys. **62**, 188 (1965); **62**, 199 (1965); **62**, 211 (1965).
[22] P. Ring and P. Schuck, *The Nuclear Many-Body Problem* (Springer-Verlag, New York, 1980).
[23] J. G. Hirsch, O. Civitarese, and M. Reboiro, Phys. Rev. C **60**, 024309 (1999).
[24] F. T. Arecchi, E. Courtens, R. Gilmore, and H. Thomas, Phys. Rev. A **6**, 2211 (1972).
[25] V. V. Dodonov, I. A. Malkin, and V. I. Man'ko, Physica (Amsterdam) **72**, 597 (1974).
[26] O. Castaños, E. López-Moreno, and R. López-Peña, Rev. Mex. Fis. **49 S4**, 15 (2003).
[27] P. Kramer and M. Saraceno, *Geometry of the Time-Dependent Variational Principle in Quantum Mechanics* (Springer-Verlag, New York, 1981), Vol. 140.
[28] R. P. Feynman, Phys. Rev. **84**, 108 (1951); H. Kuratsuji and T. Suzuki, J. Math. Phys. **21**, 472 (1980).
[29] J.-P. Eckmann and D. Ruelle, Rev. Mod. Phys. **57**, 617 (1985).